Journal of Computational and Applied Mathematics 272 (2014) 350–361

Contents lists available at ScienceDirect

Journal of Computational and Applied Mathematics

journal homepage: www.elsevier.com/locate/cam

Eigenvalue solvers for three dimensional photonic crystals with face-centered cubic lattice

Tsung-Ming Huang [a], Han-En Hsieh [b], Wen-Wei Lin [c], Weichung Wang [d,*]

[a] Department of Mathematics, National Taiwan Normal University, Taipei 116, Taiwan

[b] Department of Mathematics, National Taiwan University, Taipei 106, Taiwan

[c] Department of Applied Mathematics, National Chiao Tung University, Hsinchu 300, Taiwan

[d] Institute of Applied Mathematical Sciences, National Taiwan University, Taipei 106, Taiwan

ARTICLE INFO

Article history:
Received 30 October 2012
Received in revised form 3 January 2014

Keywords:
Maxwell's equations
Three-dimensional photonic crystals
Face-centered cubic lattice
Null space free eigenvalue problem
Shift-invert residual Arnoldi method
Fast Fourier transform matrix–vector multiplications

ABSTRACT

To numerically determine the band structure of three-dimensional photonic crystals with face-centered cubic lattices, we study how the associated large-scale generalized eigenvalue problem (GEP) can be solved efficiently. The main computational challenge is due to the complexity of the coefficient matrix and the fact that the desired eigenvalues are interior. For solving the GEP by the shift-and-invert Lanczos method, we propose a preconditioning for the associated linear system therein. Recently, a way to reformat the GEP to the null space free eigenvalue problem (NFEP) is proposed. For solving the NFEP, we analyze potential advantages and disadvantages of the null space free inverse Lanczos method, the shift–invert residual Arnoldi method, and the Jacobi–Davidson method from theoretical viewpoints. These four approaches are compared numerically to find out their properties. The numerical results suggest that the shift–invert residual Arnoldi method with an initialization scheme is the fastest and the most robust eigensolver for the target eigenvalue problems. Our findings promise to play an essential role in simulating photonic crystals.

© 2014 Elsevier B.V. All rights reserved.

1. Introduction

Photonic crystals are made up of position-dependent dielectric materials with periodic structures. Depending on the shapes and permittivities of the dielectric materials, photonic crystals produce band-gaps for various frequency regions. Photonic crystals with specific band structures are of practical interest and have been extensively studied over the past few decades [1–4]. In this paper, we consider a three-dimensional (3D) photonic crystal with a face-centered cubic (FCC) lattice as shown in Fig. 1(a). Three-dimension FCC structure permits a full and complete photonic band gap rather than a pseudogap. The light with designated frequencies from any directions can be trapped in this structure [5]. A manufacturing process of 3D photonic crystal associated with the FCC lattice to emerge into the complete photonic band gap in a realistic experiment is proposed in [6]. Photonic crystals with an FCC lattice lead to a larger photonic band-gap for lower time-frequencies [7]. Such lattice structure results in many innovative applications [8,1,9,10].

To study a photonic crystal with FCC lattice numerically, we need to solve the Maxwell equations that determine the shape of the Bloch wave equations of the time-harmonic electric fields and magnetic fields of photonic crystals. In order to

* Corresponding author.
E-mail addresses: min@ntnu.edu.tw (T.-M. Huang), d99221002@ntu.edu.tw (H.-E. Hsieh), wwlin@math.nctu.edu.tw (W.-W. Lin), wwang@ntu.edu.tw (W. Wang).

http://dx.doi.org/10.1016/j.cam.2014.02.016
0377-0427/© 2014 Elsevier B.V. All rights reserved.

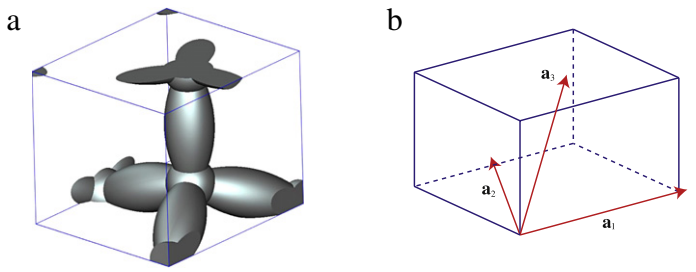

Fig. 1. The figure shows (a) schema and (b) lattice vectors of a face-centered cubic (FCC) photonic crystal structure in a primitive cell.

solve the equations, we can substitute the magnetic field by the electric field and then discretize the equations to obtain a large-scale generalized eigenvalue problem (GEP) $A\mathbf{v} = \lambda B\mathbf{v}$. The matrix A is the discrete double curl operator and it is Hermitian and positive semi-definite. B is the positive and diagonal matrix. It is important to note that the matrix B influences the spectrum of the GEP and thus the band structure of the corresponding photonic crystals. In [7], several different structures of photonic crystal are considered. The corresponding band structures have significant difference from each other.

However, solving the GEP associated with the FCC lattice is challenging. Because the dimension of the null space of A is one third of the dimension of A, it is hard to find the smallest positive eigenvalues that are of interest [7,11,12]. Another difficulty is due to the non-orthogonal FCC lattice vectors shown in Fig. 1(b). Photonic crystal with simple cubic (SC) lattice is considered in [13]. Because the eigenvectors of the discrete double curl operator associated with the SC lattice are mutually *independent* (due to the pairwise orthogonal SC lattice vectors), standard FFT can be applied to solve the corresponding eigenvalue problems. However, such eigenvectors associated with the FCC lattice are mutually *dependent* (due to the pairwise non-orthogonal FCC lattice vectors). Standard FFT techniques cannot be applied to these periodic coupling eigenvectors. A recent theoretical study [12] overcomes these difficulties by deflating the zero eigenvalues and proposing FFT-based matrix–vector multiplications via the eigendecomposition of A. While the preliminary numerical results shown in [12] is promising, how different eigensolvers perform in a computational scenario remains to be elucidated. This article fills the gap by making the following contributions.

- To solve the GEP by the shift-and-invert Lanczos method, we proposed a preconditioning scheme for the shifted linear system in the eigensolver.
- To solve the null space free eigenvalue problem, we analyze theoretically the advantages and potential disadvantages of the inverse Lanczos method, the shift–invert residual Arnoldi method, and the Jacobi–Davidson method.
- We conduct extensive numerical experiments to explore the numerical properties in timing and iteration numbers of the eigensolvers. The numerical results suggest that the shift–invert residual Arnoldi method with an initialization scheme is the fastest and the most robust eigensolver for the target eigenvalue problems.

This paper is outlined as follows: in Section 2, we briefly describe the Maxwell equations and the eigendecomposition of the degenerate coefficient matrix A. One set of orthogonal bases of the range space of A and one set of orthogonal bases of the null space of A are introduced. The null space free eigenvalue problem is derived. In Section 3, we discuss four eigenvalue solvers considered in this article. In Section 4, these eigenvalue problem solvers are compared numerically with respect to the internal linear system and the outer GEP. We conclude the paper in Section 5.

Throughout this paper, we denote the transpose and the conjugate transpose of a matrix by the superscripts $\top$ and $*$, respectively. For the matrix operations, we denote the Kronecker product of two matrices as $\otimes$. We denote the imaginary number $\sqrt{-1}$ by $\imath$ and the identity matrix of order n by I_n. The conjugate of a complex scalar $z \in \mathbb{C}$ and a complex vector $\mathbf{z} \in \mathbb{C}^n$ are represented by $\bar{z}$ and $\bar{\mathbf{z}}$, respectively.

2. Maxwell's equations and the eigenvalue problems

2.1. Maxwell's equations

The governing Maxwell's equations of a photonic crystal can be written as

$$\begin{cases} \nabla \times H = \imath\omega\varepsilon E, \\ \nabla \times E = -\imath\omega\mu_0 H, \\ \nabla \cdot (\varepsilon E) = 0, \qquad \nabla \cdot (H) = 0. \end{cases} \tag{1}$$

Here, H and E are the magnetic fields and electric fields, respectively; ω is the frequency; μ_0 is the magnetic constant and ε is the material dependent permittivity. Letting $\lambda = \mu_0\omega^2$ and eliminating the magnetic field H in (1), we have the differential eigenvalue problem

$$\nabla \times \nabla \times E = \lambda\varepsilon E, \tag{2a}$$

$$\nabla \cdot (\varepsilon E) = 0. \tag{2b}$$

The degenerate elliptic operator $\nabla\times\nabla\times$ in (2a) is self-adjoint and non-negative. Eq. (2a) is an elliptic interface problem and Eq. (2b) serves as a constraint for the degenerate elliptic Eq. (2a). Furthermore, Eq. (2b) is redundant for nonzero eigenvalues $\lambda \neq 0$ as a consequence of the calculus identity $\nabla\cdot\nabla\times \equiv 0$.

Based on the Bloch Theorem [14], the spectrum corresponding to the periodic structure in the full space is equivalent to the union of all spectra corresponding to the quasi-periodic problems in one primitive cell. We thus aim to find the Bloch eigenfunctions E for (2) satisfying the quasi-periodic condition $E(\mathbf{x}+\mathbf{a}_\ell) = e^{i2\pi\mathbf{k}\cdot\mathbf{a}_\ell}E(\mathbf{x})$, for $\ell = 1, 2, 3$. Here, $2\pi\mathbf{k}$ is the Bloch wave vector in the first Brillouin zone [3] and $\mathbf{a}_\ell$'s are the lattice translation vectors that span the primitive cell, which extends periodically to form the photonic crystals. The FCC lattice vectors are $\mathbf{a}_1 = \frac{a}{\sqrt{2}}[1,0,0]^\top$, $\mathbf{a}_2 = \frac{a}{\sqrt{2}}\left[\frac{1}{2}, \frac{\sqrt{3}}{2}, 0\right]^\top$, $\mathbf{a}_3 = \frac{a}{\sqrt{2}}\left[\frac{1}{2}, \frac{1}{2\sqrt{3}}, \sqrt{\frac{2}{3}}\right]^\top$, where a is the lattice constant. Any pairwise angles formed by $\mathbf{a}_1$, $\mathbf{a}_2$ and $\mathbf{a}_3$ measure $\pi/3$.

2.2. Discretization and the resulting eigenvalue problem

We use Yee's scheme [15] to discretize the Maxwell's equation (2) with the FCC lattice. The discretization results in a large-scale GEP

$$A\mathbf{v} = \lambda B\mathbf{v}, \tag{3}$$

where A is Hermitian and positive semi-definite for the discrete double-curl operator $\nabla\times\nabla\times$ [12], and B is positive and diagonal for the material-dependent dielectric constants [13]. Because of $\nabla\cdot\nabla\times\equiv 0$, the matrix A has many zeros that are not of interest. Derivation details of the discretization can be found in [16]. Based on these explicit matrix formulations, the eigendecompositions are derived in [12] and are briefly summarized in Section 2.3. The eigendecomposition and problem properties are used to develop the null-space free eigenvalue problem in the next section.

Let n_1, n_2, n_3 be the numbers of grid points on the x-, y- and z-axis, respectively. We assume that these numbers are the multiples of 6 and $n = n_1n_2n_3$. The mesh length on the x-, y- and z-axis are denoted by δ_x, δ_y and δ_z, respectively. The $3n\times 3n$ Hermitian matrix A in (3) is of the form

$$A = C^*C, \tag{4}$$

where

$$C = \begin{bmatrix} 0 & -C_3 & C_2 \\ C_3 & 0 & -C_1 \\ -C_2 & C_1 & 0 \end{bmatrix} \tag{5}$$

and

$$C_1 = I_{n_2n_3}\otimes K_1, \qquad C_2 = I_{n_3}\otimes K_2, \qquad C_3 = K_3. \tag{6}$$

See [12] for the definitions of the pseudo periodical matrices K_1, K_2, and K_3.

2.3. Eigendecompositions

We now briefly summarize the theoretical results introduced in [12]. The definitions of the notations used in the theories below can be found in [12]. Theorems 1 and 2 assert the Schur decompositions of C_ℓ's (for $\ell = 1, 2, 3$) and A, respectively.

Theorem 1 (*Schur Decomposition of C_ℓ's [12]*). *Let C_ℓ ($\ell = 1, 2, 3$) be defined in (6). Then,* (i) $C_i^*C_j = C_jC_i^*$, $C_iC_j = C_jC_i$, *for* $i, j = 1, 2, 3$; (ii) *C_ℓ's can be diagonalized by the same unitary matrix T:*

$$C_1T = T\Lambda_{\mathbf{x}}, \qquad C_2T = T\Lambda_{\mathbf{y}}, \quad \text{and} \quad C_3T = T\Lambda_{\mathbf{z}}, \tag{7}$$

where Λ_x, Λ_y, and Λ_z are diagonal matrices.

Theorem 2 (*Schur Decomposition of A [12]*). *Let A and $(\Lambda_{\mathbf{x}}, \Lambda_{\mathbf{y}}, \Lambda_{\mathbf{z}}, T)$ be defined in (4) and (7), respectively. Then we have*

$$Q^*AQ = \operatorname{diag}\left(0, \Lambda_q, \Lambda_q\right), \tag{8}$$

where

$$Q = (I_3\otimes T)\begin{bmatrix} \Lambda_0 & \Lambda \end{bmatrix} \equiv (I_3\otimes T)\left[\begin{array}{c|cc} \ddots & \ddots & \ddots \\ \ddots & \ddots & \ddots \\ \ddots & \ddots & \ddots \end{array}\right]$$

is unitary, $\Lambda_q = \Lambda_{\mathbf{x}}^*\Lambda_{\mathbf{x}} + \Lambda_{\mathbf{y}}^*\Lambda_{\mathbf{y}} + \Lambda_{\mathbf{z}}^*\Lambda_{\mathbf{z}}$, Λ_0 is a 3×1 block diagonal matrix, and Λ is a 3×2 block diagonal matrix.

2.4. The null space free eigenvalue problem

Theorem 2 establishes a key step to transform the GEP in (3) to the following null space free eigenvalue problem (NFEP)

$$A_r\mathbf{u} = \lambda\mathbf{u} \tag{9}$$

where

$$A_r = \Lambda_r^{\frac{1}{2}} Q_r^* B^{-1} Q_r \Lambda_r^{\frac{1}{2}} \quad \text{and} \quad \mathbf{u} = \Lambda_r^{-\frac{1}{2}} Q_r^* B\mathbf{v}.$$

In addition,

$$Q_r = (I_3 \otimes T)\, \Lambda \quad \text{and} \quad \Lambda_r = \operatorname{diag}\left(\Lambda_q, \Lambda_q\right).$$

The transformation from the GEP to the NFEP has been shown in [12]. We assert the results with a simpler proof in the following theorem.

Theorem 3. *Let T and (Λ_q, Λ) be defined in Theorems 1 and 2. Then we have*

$$\operatorname{span}\left\{B^{-1}Q_r\Lambda_r^{\frac{1}{2}}\right\} = \{x \mid Ax = \lambda Bx,\ \lambda > 0\} \tag{10}$$

and

$$\{\lambda \mid Ax = \lambda Bx,\ \lambda > 0\} = \{\lambda \mid A_r y = \lambda y\}. \tag{11}$$

Proof. From Theorem 2, it holds that $A = Q_r \Lambda_r Q_r^*$. The fact implies that

$$\left(B^{-1}A\right)\left(B^{-1}Q_r\Lambda_r^{1/2}\right) = \left(B^{-1}Q_r\Lambda_r Q_r^*\right)\left(B^{-1}Q_r\Lambda_r^{1/2}\right) = \left(B^{-1}Q_r\Lambda_r^{1/2}\right)A_r.$$

We thus obtain that $\operatorname{span}\{B^{-1}Q_r\Lambda_r^{1/2}\}$ is an invariant subspace of $B^{-1}A$ associated with the eigenvalues of A_r. Since A_r is a positive definite matrix with rank $2n$, the results in (10) and (11) hold. □

Theorem 3 shows how we can transform the GEP (3) (with dimension $3n$) to the NFEP (9) (with dimension $2n$). In particular, the zero eigenvalues of the GEP are deflated and the nonzero (positive) eigenvalues are kept without changing in NFEP. Solving the NFEP (9), rather than the GEP (3), for the wanted eigenvalues has several advantages.

- The NFEP (9) contains $2n$ positive eigenvalues. These positive eigenvalues are also the eigenvalues of the GEP (3), while the GEP has another n zero eigenvalues. Consequently, we can use an iterative eigensolver (e.g., the inverse Lanczos method and Jacobi–Davidson method) to find the smallest positive eigenvalues of the NFEP without being affected by the zero eigenvalues of (3).
- At each iteration for solving (9), we need to solve the linear system

$$\left(\Lambda_r^{1/2}Q_r^*B^{-1}Q_r\Lambda_r^{1/2} - \sigma I\right)\mathbf{y} = \mathbf{c} \tag{12}$$

for certain vectors $\mathbf{y}$ and $\mathbf{c}$ and a given shift σ. The matrix $Q_r^*B^{-1}Q_r$ is well-conditioned because $\kappa(Q_r^*B^{-1}Q_r) \le \kappa(B)$ [12] and $\kappa(B) = 13$ in the target photonic crystal setting. This fact implies that the linear system (12) with $\sigma = 0$ can be solved efficiently *without* preconditioning. More numerical details will be presented in Section 4.

2.5. Remarks about projection methods

From Theorem 2, we can see that the GEP (3) has n zero eigenvalues. It is natural to project the search space (or the search vectors) to the space that is orthogonal to the null space in each iteration. So that we can remove the components within the null space. However, such approach needs more and more computational cost to perform the orthogonal projections along the iterations, because the dimension of the search space keeps growing.

Another projection method is proposed in [7]. This method applies inverse iteration to compute the target eigenpairs. The main idea of the method is to rewrite the GEP (3) as a standard eigenvalue problem $\widetilde{A}\tilde{\mathbf{v}} = \lambda\tilde{\mathbf{v}}$ for $\widetilde{A} = B^{-1/2}AB^{-1/2}$ and $\tilde{\mathbf{v}} = B^{1/2}\mathbf{v}$ and let $\mathbf{z}$ be a null vector of $\widetilde{A}$. Then by the Hermitian property of A, it holds that $0 = \tilde{\mathbf{v}}^*\widetilde{A}\mathbf{z} = \mathbf{z}^*(\widetilde{A}\tilde{\mathbf{v}})$ which indicates that $\widetilde{A}\tilde{\mathbf{v}}$ is orthogonal to $\mathbf{z}$. Consequently, we can multiply $\tilde{\mathbf{y}}$ by $\widetilde{A}$ to eliminate the components of the null space and thus keep the iterative solutions falling into the range space of $\widetilde{A}$. However, this method exhibits oscillatory behavior. Instead of multiplying $\tilde{\mathbf{v}}$ by $\widetilde{A}$ directly, a conjugate gradient projection method with multigrid acceleration is used in [7] to compute the vector $\mathbf{w}$ by minimizing the objective function $\|\widetilde{A}\mathbf{w} - \tilde{\mathbf{v}}\|^2$, i.e., by solving the normal equation

$$(\widetilde{A}^*\widetilde{A})\mathbf{w} = (\widetilde{A}^*\tilde{\mathbf{v}}). \tag{13}$$

Unlike these projection methods, we can explicitly define the invariant subspace of $A\mathbf{v} = \lambda B\mathbf{v}$ corresponding to all nonzero eigenvalues via Theorem 3. Therefore, the positive eigenvalues of $A\mathbf{v} = \lambda B\mathbf{v}$ can be found by solving the NFEP (9) without any projection by using this invariant subspace, as the NFEP is a null space free eigenvalue problem. Comparing the methods based on the NFEP with the projection method proposed in [7], we can see the following: (i) the coefficient matrix of the linear systems in (12) is Hermitian positive definite and well-conditioned (as $\sigma = 0$ in our case). Consequently, (12)

can be solved efficiently without preconditioning. In contrast, the coefficient matrix $\widetilde{A}^*\widetilde{A}$ in (13) is not Hermitian positive definite and it needs an preconditioner; (ii) the NFEP (9) can be solved by subspace iterative eigensolvers. These eigensolvers usually converge faster than the inverse iteration method; (iii) the null space does not affect the convergence behavior of the eigensolver for solving (9); however, the null space will downgrade the convergence of the projection method.

3. The eigenvalue solvers

In this section, we discuss how we can solve the GEP (3) or the NFEP (9) by using different eigenvalue solvers and their advantages.

3.1. Shift-and-invert Lanczos method (SILM) for the GEP (3)

The Shift-and-invert Lanczos Method (SILM) can be used to find a few of the (interior) smallest positive eigenvalues of the GEP (3). In the SILM, a standard Lanczos method is used to solve the shifted-and-inverted eigenvalue problem

$$\mathbb{A}_s\mathbf{v} = \mu\mathbf{v}, \tag{14}$$

where $\mathbb{A}_s = (A - \sigma B)^{-1}B$, $\mu = (\lambda - \sigma)^{-1}$, and σ is the shift. The most expensive part of the SILM is to solve the shifted linear system

$$(A - \sigma B)\mathbf{z} = \mathbf{b}, \tag{15}$$

where $\mathbf{b}$ and $\mathbf{z}$ are intermediate vectors.

To solve the linear system (15), we propose a preconditioning scheme motivated by the eigendecomposition $A = Q\Lambda Q^*$ in (8). Here, the matrix Q is unitary and B is a diagonal matrix. By using the eigendecomposition and averaging the diagonal entries of B, we have the preconditioner

$$M = A - \tau I = Q\Lambda Q^* - \tau I = Q(\Lambda - \tau I)Q^*, \tag{16}$$

where $\tau = \sigma\varepsilon_0$ and ε_0 is the average of the diagonal entries of B. The following facts illustrate why M can be an efficient preconditioner.

- While there is an efficient way [12] to compute the matrix–vector multiplications $Q^*\mathbf{d}$ and $Q\mathbf{e}$ for $M^{-1}\mathbf{d} = [Q(\Lambda - \tau I)^{-1}Q^*]\mathbf{d}$, we can further accelerate the computation of $M^{-1}\mathbf{d}$. Our idea is to use the Schur decompositions of C_ℓ's in Theorem 1 to solve the linear system

  $$(A - \tau I)\mathbf{y} = \mathbf{d} \tag{17}$$

  as the following.

  From (5), it holds that

  $$A = I_3 \otimes \left(G^*G\right) - GG^*,$$

  where $G = [C_1^\top, C_2^\top, C_3^\top]^\top$ and Eq. (17) can be reformulated as

  $$\left\{I_3 \otimes \left(G^*G\right) - \tau I\right\}\mathbf{y} = \mathbf{d} + GG^*\mathbf{y}. \tag{18}$$

  Multiplying (17) by GG^* and applying the fact $CG = 0$, we have $GG^*\mathbf{y} = -\tau^{-1}GG^*\mathbf{d}$ and Eq. (18) becomes

  $$\left\{I_3 \otimes \left(G^*G\right) - \tau I\right\}\mathbf{y} = \mathbf{d} - \tau^{-1}GG^*\mathbf{d}. \tag{19}$$

  Applying the Schur decompositions of C_ℓ's in Theorem 1, the solution $\mathbf{y}$ in (19) can be computed by

  $$\left(I_3 \otimes \Lambda_q - \tau I\right)\tilde{\mathbf{y}} = \left(I - \tau^{-1}\begin{bmatrix}\Lambda_{\mathbf{x}}\\ \Lambda_{\mathbf{y}}\\ \Lambda_{\mathbf{z}}\end{bmatrix}\begin{bmatrix}\Lambda_{\mathbf{x}}^* & \Lambda_{\mathbf{y}}^* & \Lambda_{\mathbf{z}}^*\end{bmatrix}\right)(I_3 \otimes T)^*\,\mathbf{d} \equiv \tilde{\mathbf{d}}$$

  and

  $$\mathbf{y} = (I_3 \otimes T)\,\tilde{\mathbf{y}}.$$

  As Λ_q, Λ_x, Λ_y, and Λ_z are all diagonal matrices, the main computational cost for solving $\mathbf{y}$ is the matrix–vector multiplications $T^*\mathbf{p}$ and $T\mathbf{q}$. As shown in [12], these two matrix–vector multiplications can be computed efficiently by the FFT-based schemes and therefore the preconditioning linear system (17) can be solved efficiently.
- We can rewrite the linear system (15) as

  $$A_M\mathbf{z} = \tilde{\mathbf{b}}, \tag{20}$$

  where $A_M = M^{-1}(A - \sigma B) = I + \sigma M^{-1}(\varepsilon_0 I - B)$ and $\tilde{\mathbf{b}} = M^{-1}\mathbf{b}$. If we solve the linear system (15) with preconditioner M by an iterative method, we need to compute the matrix–vector multiplication involving A and solve linear system (17) at each iteration. Alternatively, if we solve the rewritten system (20) by an iterative method, we only need to compute $\mathbf{t} + \sigma M^{-1}(\varepsilon_0 I - B)\mathbf{t}$ at each iteration for a given vector $\mathbf{t}$. This alternative approach is cheaper, because we only need to solve (17) and there is no need to compute the matrix–vector multiplication involving A.

The aforementioned preconditioning schemes are different from existed approaches in the following sense.

- Both of the preconditioners proposed in [13] for the SC lattice and the preconditioner suggested in (16) for the FCC lattice have the form $A - \tau I$. However, they are derived from completely different ways. In the SC lattice, the pairwise angles formed by the lattice vectors are $\pi/2$. So we can rewrite the eigenvalue problem (2a) containing the double curl operator $\nabla \times \nabla$ in another form that contains the Laplace operator ∇^2. Consequently, the linear system due to the discretization of the Laplace operator can be solved by FFT efficiently. However, this derivation cannot be applied to the FCC lattice because of the particular FCC periodicity formulation. Instead, the derivation of the preconditioner here is based on the explicit eigendecompositions of C_ℓ and A given in Theorem 1 and (8), respectively. Without this eigendecomposition, we would not be able to find the aforementioned way to solve the preconditioner linear system (17).
- The approach based on the preconditioned linear system (20) can be viewed as an improvement of the scheme proposed in [13] with a saving of matrix–vector multiplication involving A.

3.2. Null space free Lanczos method (NFLM) for the NFEP (9)

The SILM needs a pre-determined shift σ as shown in Eq. (14). However, it is not easy to choose a suitable shift value to gain efficiency of overall computation a priori. Alternatively, as discussed in Section 2.4, we can use inverse Lanczos method (no shift is needed) to solve the NFEP (9), because the NFEP has no zero eigenvalue. We call the approach as the Null-space Free Lanczos Method (NFLM) and it is used to find the wanted eigenvalues of the GEP (3).

3.3. Shift–invert residual Arnoldi method (SIRA) and Jacobi–Davidson method (JD) for the NFEP (9)

We consider other methods, namely the shift–invert residual Arnoldi method and the Jacobi–Davidson method, to solve the NFEP (9).

The residual Arnoldi method (RA) has been proposed to solve the eigenvalue problem $\mathbb{A}x = \lambda x$ and it is mathematically equivalent to the Arnoldi method in exact arithmetic [17,18]. To obtain the next Krylov basis v_{m+1} in the RA, the residual $r = \mathbb{A}y - \theta y$ is orthogonalized against to an orthonormal basis of the m-dimensional Krylov subspace $V_m = [v_1, \ldots, v_m]$. Here, (θ, y) is the Ritz pair of $\mathbb{A}$ with respect to V_m and the m-dimensional Krylov subspace is constructed by the Arnoldi process. The RA can be extended to solve the eigenvalue problem $(\mathbb{A} - \sigma I)^{-1}x = (\lambda - \sigma)x$ and this variant of RA is named as the Shift–Invert Residual Arnoldi method (SIRA). The SIRA is designed to find a few of eigenpairs that are close to the shift value σ for the eigenvalue problem $\mathbb{A}x = \lambda x$ [19,17,18]. To compute the basis vector in each iteration of the SIRA, the method first solves the linear system

$$(\mathbb{A} - \sigma I)\, u = r \tag{21}$$

for the residual vector $r = \mathbb{A}y - \theta y$. The basis vector v_{m+1} is then computed by orthogonalizing u against V_m. In practical, the SIRA is usually realized as the *inexact* SIRA, in which the linear system (21) is solved approximately [17,18]. Jia and Li [19] have proved that the inexact SIRA mimics the exact SIRA well when the relative error of the approximate solution of (21) is modestly small (around $[10^{-4}, 10^{-3}]$) at each iteration.

Jacobi–Davidson method (JD), on the other hand, is also an inexact eigenvalue solver [20]. In each of the JD iteration, the correction equation

$$\left(I - uu^*\right)(\mathbb{A} - \theta I)\left(I - uu^*\right) t = -r \tag{22}$$

is solved approximately by an iterative solver. In a one step local analysis [19], the SIRA and JD are shown to be mathematically equivalent if the two problems (21) and (22) are solved exactly. Based on the local analysis, a new version of the inexact SIRA that shares the same framework with the JD has been proposed in [19]. While there are various ways to describe and implement the SIRA and JD algorithms, we use the version given in Algorithm 1 to solve the NFEP $A_r\mathbf{u} = \lambda\mathbf{u}$ in (9). As demonstrated in the algorithm, the only difference between the two methods is that the SIRA solves the linear system (23) and the JD solves the correction equation (24) (both approximately).

We highlight some properties of the SIRA as follows.

- *Eigenvalue deflation is embedded implicitly for the SIRA*. In the outer iteration of Algorithm 1 (line 13), the vector t_k is orthogonalized against $\mathbb{V}_x$. Because the columns of $\mathbb{V}_x$ are the convergent eigenvectors and pairwise orthogonal (as A_r is Hermitian), the convergent eigenvalues are thus automatically deflated from the subspace span$\{\mathbb{V}_{k+1}\}$.
- *There is no need to perform shift in the SIRA and we can set* $\sigma = 0$ *in* (23). In the jth iteration of Algorithm 1, the first smallest $(j-1)$ eigenvalues are found and deflated. The jth smallest positive eigenvalue thus becomes the smallest positive eigenvalue in the jth iteration, as A_r is positive definite. Consequently, the shift value σ can be set to zero. The coefficient matrix of the linear system in (23) becomes A_r and it is Hermitian positive definite. We can thus use the conjugate gradient method to solve (23). This is an advantage for taking $\sigma = 0$, otherwise the matrix $(A_r - \sigma I)$ may be indefinite for some positive σ's.
- *The resulting linear system is well-conditioned*. By setting $\sigma = 0$, the linear system (23) has the form $A_r t_k = r_k$. The condition number of A_r is less than or equal to the ratio $\varepsilon_i/\varepsilon_o$ [12]. In particular, the ratio equals to 13 in our numerical experiments. That is, the condition number of A_r is as small as 13 and this small condition number property is independent to the matrix size. The fact also suggests that the convergence of the conjugate gradient method is fast.

Algorithm 1 The Shift–Invert Residual Arnoldi method and the Jacobi–Davidson method for solving $A_r x = \lambda x$.

Input: Hermitian coefficient matrix A_r, the number of desired eigenvalues ℓ, an initial vector $\mathbb{V}_1$, target σ, tolerances ε and number of Ritz vectors m.

Output: The desired eigenpairs (λ_j, x_j) for $j = 1, \ldots, \ell$.

1: Set $\mathbb{V}_x = [\,]$, $k = 1$ and $r_0 = e_1$.
2: **for** $j = 1, \ldots, \ell$ **do**
3: Compute $\mathbb{W}_k = A_r \mathbb{V}_k$ and $\mathbb{M}_k = \mathbb{V}_k^* \mathbb{W}_k$.
4: **while** ($\|r_{k-1}\|_2 \geq \varepsilon$) **do**
5: Compute the eigenpairs (θ_i, s_i) of $\mathbb{M}_k s = \theta s$ with $\|s_i\|_2 = 1$ and $\sigma < \theta_1 \leq \theta_2 \leq \cdots$.
6: Compute $u_k = \mathbb{V}_k s_1$ and $r_k = (A_r - \theta_1 I) u_k$.
7: **if** ($\|r_k\|_2 < \varepsilon$), set $\lambda_j = \theta_1$, $x_j = u_k$, $k := k + 1$. Go to line 4.
8: **if** (use Shift–Invert Residual Arnoldi method) **then**
9: Solve (approximately) a t_k from
$$(A_r - \sigma I) t_k = r_k. \tag{23}$$
10: **else if** (use Jacobi–Davidson method) **then**
11: Solve (approximately) a $t_k \perp u_k$ from
$$\left(I - u_k u_k^*\right)(A_r - \theta_1 I)\left(I - u_k u_k^*\right) t_k = -r_k. \tag{24}$$
12: **end if**
13: Orthogonalize t_k against $[\mathbb{V}_x\ \mathbb{V}_k]$; set $v_{k+1} = t_k / \|t_k\|$.
14: Compute $w_{k+1} = A_r v_{k+1}$, $\mathbb{M}_{k+1} = \begin{bmatrix} \mathbb{M}_k & \mathbb{V}_k^* w_{k+1} \\ v_{k+1}^* \mathbb{W}_k & v_{k+1}^* w_{k+1} \end{bmatrix}$.
15: Expand $\mathbb{V}_{k+1} = [\mathbb{V}_k, v_{k+1}]$ and $\mathbb{W}_{k+1} = [\mathbb{W}_k, w_{k+1}]$. Set $k := k + 1$.
16: **end while**
17: Set $\mathbb{V}_x = [\mathbb{V}_x, x_j]$, $\mathbb{V}_{m-1} = \mathbb{V}_{k-1}[s_2, \cdots, s_m]$, $k = m - 1$ and $r_{k-1} = e_1$.
18: **end for**

- *There is a good way to choose the initial searching subspace*. We need to solve a sequence of eigenvalue problems associated with various **k**'s to plot the band structure diagram. For two eigenvalue problems associated with slightly different **k**'s, we can solve one eigenvalue problem first and then use the convergent eigenvectors as the initial guesses of the other eigenvalue problem to improve the convergence.

As the SIRA and JD have the same framework, the JD also shares the good properties in embedded eigenvalue deflation and the initialization scheme. However, the difficulties to solve the linear system (23) in the SIRA and the correction equation (24) in the JD are quite different. For the SIRA, the linear system (23) can be efficiently solved by an iterative method *without* any preconditioner as $\kappa(A_r) = 13$ in our numerical setting. For example, it takes only 37 iterations to solve a 3,456,000 × 3,456,000 testing problem by the CG method with stopping tolerance 6.4×10^{-15}. However, it is not easy to find an efficient preconditioner for the correction equation (24) in the JD directly. Therefore, we rewrite (24) as

$$(A_r - \theta_1 I)\, t_k = -r_k + \eta u_k$$

and compute

$$t_k = t_1 + \eta t_2 \quad \text{with } \eta = -\frac{u_k^* t_1}{u_k^* t_2}.$$

Here, t_1 and t_2 are approximate solutions of

$$(A_r - \theta_1 I)\, t = -r_k \tag{25}$$

and

$$(A_r - \theta_1 I)\, t = u_k, \tag{26}$$

respectively. This scheme requires solutions of two linear systems (25) and (26) in each iteration, while only one linear system is solved in the SIRA.

3.4. A short summary

We summarize the characteristics of the GEP, NFEP, and the eigensolvers in Table 1. Furthermore, we summarize the characteristics of the eigensolvers NFLM, SIRA, and JD for solving the NFEP (9) in Table 2. We conclude this section by the following remark. The key computational kernel of the eigenvalue solvers discussed above are the matrix–vector multiplications $T^*\mathbf{p}$ and $T\mathbf{q}$ for vectors $\mathbf{p}$ and $\mathbf{q}$. An efficient algorithm for computing these matrix–vector multiplications has been proposed in [12] and we use the algorithm here.

Table 1
Characteristics for solving the GEP (3) by the SILM and the NFEP (9) by the NFLM.

	GEP (3)	NFEP (9)
Eigensolver	SILM	NFLM
Dimension	$3n \times 3n$	$2n \times 2n$
Shift	σ in (14)	No
Linear system	$A_M\mathbf{z} = \tilde{\mathbf{b}}$ in (20)	$(Q_r^* B^{-1} Q_r)\mathbf{y} = \Lambda_r^{-1/2}\mathbf{c}$ in (12)
Preconditioner	$M = A - \tau I$	Not necessary[a]
MV mult.[b]	Two for solving $M\mathbf{y} = \mathbf{d}$(17)	One for Q_r^* and Q_r in A_r

[a] The corresponding coefficient matrix $(Q_r^* B^{-1} Q_r)$ is well-conditioned.
[b] FFT-based matrix–vector multiplications $T^*\mathbf{p}$ and $T\mathbf{q}$.

Table 2
Characteristics of the eigensolvers NFLM, SIRA, and JD for solving the NFEP (9).

Eigensolver	NFLM	SIRA	JD
Shift	No	No	θ_1 in (25) and (26)
Linear system	(12)[a]	(23)[a]($\sigma = 0$)	(25) and (26)
LS accuracy	High	Inexact	Inexact
Preconditioner	Not necessary	Not necessary	Not necessary
MV mult.[b]	for Q_r^* and Q_r	for Q_r^* and Q_r	for $A_r - \theta_1 I$

[a] The corresponding coefficient matrix is $(Q_r^* B^{-1} Q_r)$ and it is well-conditioned.
[b] FFT-based matrix–vector multiplications $T^*\mathbf{p}$ and $T\mathbf{q}$.

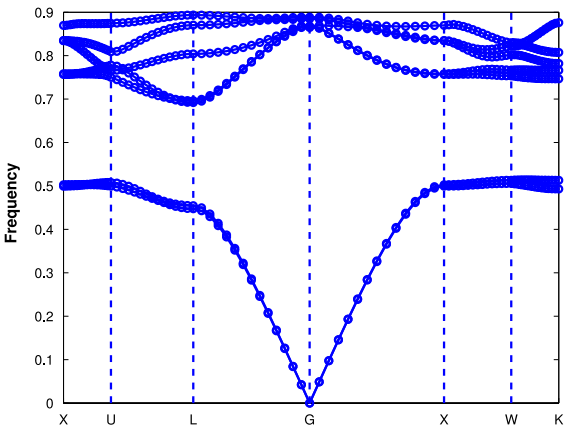

Fig. 2. The computed band structure diagram.

4. Numerical comparisons

To study the convergence behavior of the eigensolvers in terms of timing and iteration numbers, we consider the setup described in [7]. The lattice consists of dielectric spheres with a connecting spheroid as shown in Fig. 1(a). The radius r of the spheres is $r = 0.12a$ and the connecting spheroid has a minor axis length $s = 0.11a$, where a is the lattice constant. Inside the structure is the dielectric material with permittivity contrast $\varepsilon_i/\varepsilon_o = 13$. Consequently, the entries of the diagonal matrix B in (3) are either 1 or 13, which depends on the location of the grid points. The computed band structure diagram is shown in Fig. 2. The x-axis (and the dashed lines) indicates the points X, U, L, G, X, W, and K that connect the boundary of the first Brillouin zone. In each of the segments, i.e. $\overline{XU}$, $\overline{UL}$, ..., $\overline{WK}$, fifteen uniformly distributed sampling vectors $\mathbf{k}$ are chosen. The frequency $\omega = \frac{\sqrt{\lambda}}{2\pi}$ is shown on the y-axis, where λ is the eigenvalue of the GEP (3).

All computations in this section are carried out in MATLAB 2011b. In the SILM, NFLM, SIRA, and JD, we need to compute the matrix–vector multiplications $T^*\mathbf{p}$ and $T\mathbf{q}$ by FFT. For the forward FFT associated with $T^*\mathbf{p}$ is computed by `fft` in MATLAB. For the backward FFT associated with $T\mathbf{q}$ is computed by `ifft`. The MATLAB commands `tic` and `toc` are used to measure the elapsed time, and the IEEE double-precision floating-point arithmetic with $\epsilon \approx 10^{-16}$ is used. We choose $n_1 = n_2 = n_3 = 120$, and $n = n_1 n_2 n_3 = 1,728,000$. Consequently, the matrix sizes of A and A_r in (3) and (9) are 5,184,000

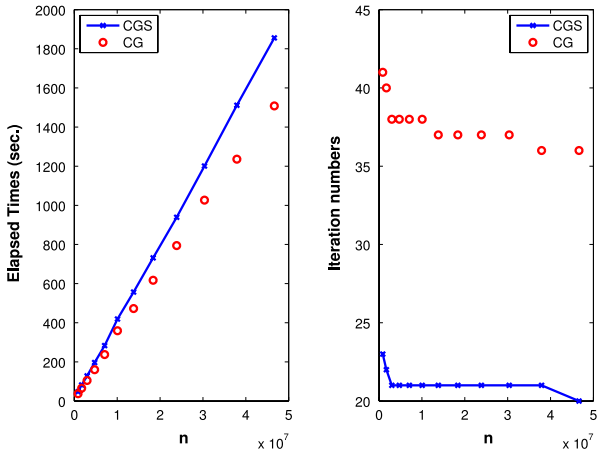

Fig. 3. The elapsed times and iteration numbers for solving the linear systems (20) and (12) by using CGS (in the SILM) and CG (in the NFLM) methods, respectively. For the mesh sizes, we take $n_1 = n_2 = n_3 = m_j$ with $m_j = 96 + 24j$ for $j = 0, 1, \ldots, 13$. The dimension $n = m_j^3$ ranges from 884,736 to 67,917,312.

(or $3n$) and 3,456,000 (or $2n$), respectively. For the hardware configuration, we use a HP workstation that is equipped with two Intel Quad-Core Xeon X5687 3.6 GHz CPUs, 48 GB of main memory, and the RedHat Linux operating system.

4.1. The linear systems in the SILM and NFLM

In Sections 4.1 and 4.2, we compare the SILM and NFLM for solving the GEP (3) and the NFEP (9), respectively. Numerical results reflect the characteristics of the GEP, NFEP, and the eigensolvers shown in Table 1.

We conduct numerical experiments to evaluate the linear system solvers. Fig. 3 shows the timing and iteration results for solving the linear systems (20) and (12). The results are obtained by the following settings. For the SILM, the MATLAB function `eigs` is used to solve the shifted-and-inverted eigenvalue problem (14) and the `cgs` (conjugate gradient squared) is used to solve the linear system $A_M\mathbf{z} = \tilde{\mathbf{b}}$ in (20) without preconditioning, as the preconditioner M has already been incorporated. For the NFLM, the `eigs` is used to solve the NFEP (9) without shifting. The MATLAB function `pcg` is used to solve the linear system $(Q_r^* B^{-1} Q_r)\mathbf{y} = \Lambda_r^{-1/2}\mathbf{c}$ defined in (12) without preconditioning. The stopping criteria for (20) and (12) are both equal to 6.4×10^{-15}.

Fig. 3(a) shows that CG (in the NFLM) takes less time to solve (12). The reasons are twofold: FFT-based matrix–vector multiplications and dimensions as shown in Table 1.

- While the iteration number of the CGS (in the SILM) is smaller; however, two matrix–vector multiplications are required in each CGS iteration. The total number of matrix–vector multiplications for the CGS is thus larger than that of the CG (in the NFLM).
- The dimensions of the coefficient matrices in the SILM and NFLM are $3n$ and $2n$, respectively. Therefore, except for the matrix–vector multiplications, the computational cost for the other operators in the CG method is less than that of the CGS method in each iteration.

Fig. 3(b) shows that the CGS (in the SILM) and CG (in the NFLM) take around 21 and 37 iterations to converge, respectively. For the problems with dimensions ranging from 884,736 to 67,917,312, the results suggest that the preconditioner in the SILM is quite effective. The results are parallel to our argument that the linear system in the NFLM is well-conditioned.

4.2. Solving the GEP and NFEP

We use the SILM and NFLM to compute the five smallest positive eigenvalues of the GEP (3) and the NFEP (9), respectively. Some details of the numerical experiments are given below. As indicated in Table 1, we need to choose the shift σ for the SILM and we use the following heuristic. In the SILM, the shift $\sigma = 2$ when the smallest positive eigenvalue is greater than 4; otherwise, it is taken as 0.01. While the shift σ affects the SILM significantly, the heuristic strategy for choosing the shift is based on our numerical experience. This strategy is not always the best choice; however, the results are reasonably close to the best choice in our experience. Based on the residual estimation bound [21], we set the stopping tolerances of the MATLAB function `eigs` in solving (3) and (9) to be $10^{-4} \times \epsilon$ and $10^{-4} \times \epsilon/(2\sqrt{\delta_x^{-2} + \delta_y^{-2} + \delta_z^{-2}})$, respectively. For each wave vector $\mathbf{k}$, we set the maximal dimension of the Krylov subspace (i.e. the restarting number) $p = 21$ to compute the five smallest positive eigenvalues.

Fig. 4 shows the iteration numbers and elapsed time for solving the eigenvalue problems corresponding to each of the $\mathbf{k}$'s with matrix dimension 3,456,000. Fig. 4(a) shows that the NFLM takes similar or less iteration numbers. For the timing

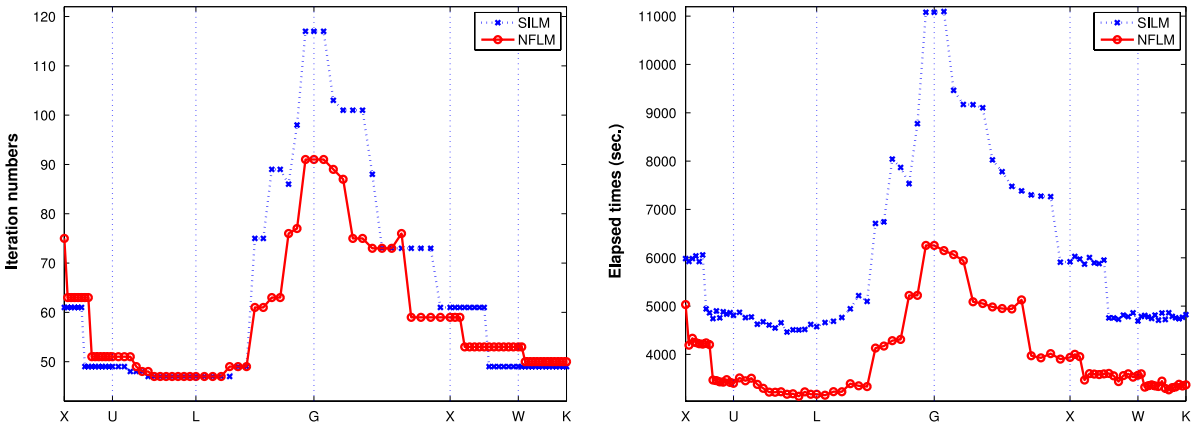

(a) Iteration numbers. (b) CPU times.

Fig. 4. Iteration numbers and elapsed times of the SILM and NFLM associated with various wave vectors $\mathbf{k}$ for solving the GEP (3) (with matrix dimension 5,184,000) and the NFEP (9) (with matrix dimension 3,456,000), respectively.

results, they are affected by the iteration numbers and the linear system solvers as discussed in Section 4.1. We have seen the iteration number results in Fig. 4(a). For the linear system solvers, Fig. 3(a) shows that CG in the NFLM takes less time to solve the linear system. Consequently, as shown in Fig. 4(b), the NFLM outperforms the SILM in timing for all tested eigenvalue problems.

Comparing Figs. 2 and 4, we can see that the band structure (or the corresponding eigenvalue spectrum) is closely related to the timing and the resulting iteration number. Both of the SILM and NFLM require more time and more iterations to converge to the eigenvalues that are closer to zero for $\mathbf{k} \approx G$. However, it is worth noting that the band structure has greater effects on the SILM, as the zero eigenvalues are deflated in the NFLM.

4.3. Solving the NFEP by the NFLM, SIRA, and JD

In this subsection, our numerical experiments focus on the comparisons of the eigensolvers NFLM, JD, and SIRA for solving the NFEP (9) (with dimension 3,456,000) and for finding the full band structure. The numerical results in timing and iteration numbers are closely related to the characteristics of these eigensolvers listed in Table 2.

The numerical results are obtained by using the following settings. The MATLAB function `minres` is used to solve (25) and (26) in each iteration of the JD method, as the coefficient matrices are Hermitian. In the `minres`, we set the stopping tolerance as 10^{-3}. The heuristic strategies in [13] are used to determine the maximal iteration number for `minres`. We take the shift value $\sigma = 0$ in the SIRA so that the MATLAB function `pcg` (without preconditioning) can be applied to solve (23). The stopping criterion for `pcg` is taken as 5×10^{-4}.

To compute the full band structure, it involves a sequence of eigenvalue problems that the successive eigenvalue problems are associated with slightly different wave vector $\mathbf{k}$. We thus have two options to choose the initial vector for the NFLM and the initial subspaces for the SIRA and JD. First, we can simply use a random vector or a random subspace for each eigenvalue problem. Second, for the single initial vector in the NFLM, we can use the smallest convergent eigenvector obtained from the previous eigenvalue problem EP_{i-1} as the initial guess of the current problem EP_i. Similarly, we use five convergent eigenvectors of the previous eigenvalue problem as the initial subspace in the SIRA and JD. While there are two options for each method, we do not have to compare all of them according to the following facts.

- The effect of the initial vector is limited to the NFLM in our numerical experience. This is because only one single vector is initialized by the convergent eigenvector. Since the NFLM performs similarly for the two initialization options, we simply use the random vector here for the NFLM.
- For the JD, we only consider using the previous convergent eigenvectors in the initialization. This is not only because the initialization scheme does improve the convergence of the JD in our numerical experience [22]. It is also because the JD needs to solve two linear systems in each iteration, while the NFLM and SIRA solves only one linear system (see Table 2), and the use of random initial guesses will have no comparison to the NFLM and SIRA.
- For the initial guesses of the SIRA, we consider the two cases that either a random initial vector (denoted as SIRA-rnd) or the aforementioned initial subspace (denoted as SIRA-prv) is used.

Fig. 5 shows the timing results for the NFLM, SIRA-rnd, SIRA-prv, and JD. Observing the figure, have the following highlights.

- The NFLM outperforms the JD for most benchmark problems, even though the JD is accelerated by the initialization scheme. This is because two linear systems (25) and (26) are solved in each iteration of the JD, while only one linear system is solved in the NFLM.

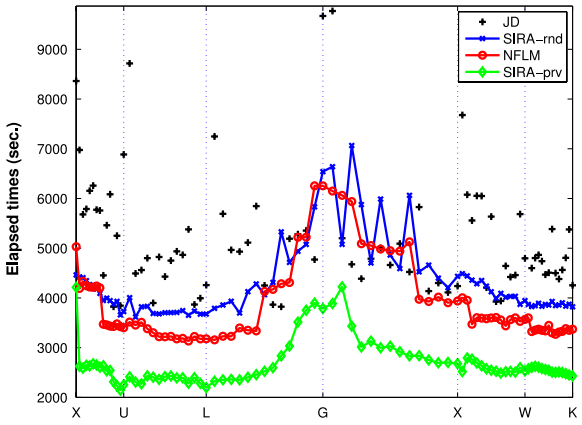

Fig. 5. Elapsed times of the NFLM, SIRA, and JD associated with various wave vectors **k**. The matrix size of A_r in (9) is 3,456,000.

Table 3
Relations between the inner and outer loops in the NFLM and SIRA.

Eigensolver	NFLM	SIRA-rnd	SIRA-prv
Median ite no in inner loop	37	10	10
Median ite no in outer loop	53	176	122
Product of the iteration numbers	1961	1760	1220

- The NFLM and SIRA-rnd perform somewhat similarly. The behavior can be understood from Table 2, because both methods need no shift, solve one linear systems, need no preconditioners, and use the FFT-based matrix–vector multiplications.
- The elapsed time for the SIRA-prv is significantly reduced from the time for the SIRA-rnd. Consequently, the SIRA-prv converges faster than the NFLM in the sequence of the eigenvalue problems.

Table 2 actually suggests a clue to understand the convergence behavior of the NFLM and SIRA from the viewpoint of the outer and inner loops. In the inner loops, the NFLM needs to solve the linear system (12) iteratively in a higher accuracy to form the Krylov subspace. In contrast, the SIRA has the luxury to converge even the solution of the linear system (23) is inexact. To study the interplay between the inner and outer loops, we list the median numbers of the iteration numbers in Table 3. The products of the iteration numbers shown in the table suggest an indicator why the NFLM and SIRA-rnd perform similarly (the product values are similar) and why the SIRA-prv is the fastest one among these three eigensolvers (the product value 1,220 is much less than others). Table 3 has shown a preliminary observation regarding the interplay between outer and inner loops in the NFLM and SIRA. However, it remains an interesting open question regarding how we can determine the accuracy requirement of the inner loop in the SIRA to achieve the minimal total run-time without downgrading the eigenpair accuracy.

5. Conclusions

Solving the eigenvalue problem arising from Yee's discretization of the three-dimensional photonic crystal with a face-centered cubic lattice is a computational challenge. We compare four eigensolvers to solve the eigenvalue problem. The shift-and-invert Lanczos method (SILM) is used to solve the original $3n \times 3n$ indefinite eigenvalue problem. Based on the theoretical framework proposed in [12], the null-space free Lanczos method (NFLM) is used to solve the reduced $2n \times 2n$ positive definite eigenvalue problem. We further consider the shift–invert residual Arnoldi method (SIRA) and Jacobi–Davidson method (JD) for solving the reduced eigenvalue problems. We have illustrated the advantages and disadvantages of the methods by providing the insights of the methods both theoretically and numerically. Among these four eigensolvers, the SIRA-prv outperforms other methods. The SIRA-prv is the most efficient solver because: (i) the method solves the $2n \times 2n$ null-space free eigenvalue problem (9) without shift nor inversion; (ii) the associated linear system (23) is well-conditioned and only approximate solution is necessary; and (iii) the key computations can be performed by FFT-based matrix–vector multiplications.

All the eigensolvers are implemented by MATLAB to illustrate their numerical properties. Based on these numerical experiments, we have identified the most efficient eigensolver. Advanced implementations based on multi-core technologies such as graphic processing unit (GPU) or parallel computers can further shorten the computational time. The solver will then be capable of solving larger problems regarding the numerical simulation of three-dimensional photonic crystals in less time.

Acknowledgments

The authors appreciate the anonymous referees for their useful comments and suggestions. This work is partially supported by the National Science Council, the Taida Institute of Mathematical Sciences, and the National Center for Theoretical Sciences in Taiwan.

References

[1] J.S. Foresi, P.R. Villeneuve, J. Ferrera, E.R. Thoen, G. Steinmeyer, S. Fan, J.D. Joannopoulos, L.C. Kimerling, H.I. Smith, E.P. Ippen, Photonic-bandgap microcavities in optical waveguides, Nature 390 (1997) 143–145.
[2] S. John, Strong localization of photons in certain disordered dielectric superlattices, Phys. Rev. Lett. 58 (1987) 2486–2489.
[3] J.D. Joannopoulos, S.G. Johnson, J.N. Winn, R.D. Meade, Photonic Crystals: Molding the Flow of Light, Princeton University Press, 2008.
[4] E. Yablonovitch, Inhibited spontaneous emission in solid-state physics and electronics, Phys. Rev. Lett. 58 (1987) 2059–2062.
[5] Eli Yablonovitch, T.J. Gmitter, Photonic band structure: the face-centered-cubic case, Phys. Rev. Lett. 63 (18) (1989) 1950.
[6] Eli Yablonovitch, T.J. Gmitter, K.M. Leung, Photonic band structure: the face-centered-cubic case employing nonspherical atoms, Phys. Rev. Lett. 67 (17) (1991) 2295.
[7] R.L. Chern, C. Chung Chang, Chien-C. Chang, R.R. Hwang, Numerical study of three-dimensional photonic crystals with large band gaps, J. Phys. Soc. Japan 73 (2004) 727–737.
[8] D.L. Bullock, C.-C. Shih, R.S. Margulies, Photonic band structure investigation of two-dimensional Bragg reflector mirrors for semiconductor laser mode control, J. Opt. Soc. Amer. B 10 (1993) 399–403.
[9] A. Mekis, J.C. Chen, I. Kurland, S. Fan, P.R. Villeneuve, J.D. Joannopoulos, High transmission through sharp bends in photonic crystal waveguides, Phys. Rev. Lett. 77 (1996) 3787–3790.
[10] O. Painter, R.K. Lee, A. Scherer, A. Yariv, J.D. O'Brien, P.D. Dapkus, I. Kim, Two-dimensional photonic band-gap defect mode laser, Science 284 (1999) 1819–1821.
[11] R. Hiptmair, K. Neymeyr, Multilevel method for mixed eigenproblems, SIAM J. Sci. Comput. 23 (2002) 2141–2164.
[12] T.-M. Huang, H.-E. Hsieh, W.-W. Lin, W. Wang, Eigendecomposition of the discrete double-curl operator with application to fast eigensolver for three-dimensional photonic crystals, SIAM J. Matrix Anal. Appl. 34 (2) (2013) 369–391.
[13] T.-M. Huang, W.-J. Chang, Y.-L. Huang, W.-W. Lin, W.-C. Wang, W. Wang, Preconditioning bandgap eigenvalue problems in three dimensional photonic crystals simulations, J. Comput. Phys. 229 (2010) 8684–8703.
[14] C. Kittel, Introduction to Solid State Physics, Wiley, New York, 2005.
[15] K. Yee, Numerical solution of initial boundary value problems involving Maxwell's equations in isotropic media, IEEE Trans. Antennas and Propagation 14 (1966) 302–307.
[16] T.-M. Huang, H.-E. Hsieh, W.-W. Lin, W. Wang, Matrix representation of the double-curl operator for simulating three dimensional photonic crystals, Math. Comput. Modelling 58 (2013) 379–392.
[17] C.-R. Lee, G.W. Stewart, Analysis of the Residual Arnoldi Method, Technical Report CS-TR-4890, Department Computer Science, University of Maryland, 2007.
[18] Che-Rung Lee, Residual Arnoldi method, theory, package and experiments, Ph.D. Thesis, University of Maryland, 2007.
[19] Z. Jia, C. Li, Inner iterations in the shift-invert residual Arnoldi method and the Jacobi–Davidson method, Sci. China Math. (2014) 1–20.
[20] G.L.G. Sleijpen, H.A. van der Vorst, A Jacobi–Davidson iteration method for linear eigenvalue problems, SIAM J. Matrix Anal. Appl. 17 (1996) 401–425.
[21] T.-M. Huang, H.-E. Hsieh, W.-W. Lin, W. Wang, Fast Lanczos Eigenvalue Solvers for Band Structures of Three Dimensional Photonic Crystals with Face-Centered Cubic Lattice, Technical Report, NCTS Preprints in Mathematics, National Tsing Hua University, Hsinchu, Taiwan, 2013-3-003, 2013.
[22] T.-M. Huang, Y.-C. Kuo, W. Wang, Computing extremal eigenvalues for three-dimensional photonic crystals with wave vectors near the Brillouin zone center, J. Sci. Comput. 55 (3) (2013) 529–551.